TRANSLATIONAL CHEMISTRY
AN INTERFACE JOURNAL
HTTPS://WWW.TRANSLATIONALCHEMISTRY.COM/

ORIGINAL ARTICLE | DOI: 10.5584/translationalchemistry.v1i1.240

Evaluation of positively charged benzothioxanthene imide derivatives as potential photosensitizers for antimicrobial photodynamic therapy

Joana Galhano,[1] Darío Puchán Sánchez,[2] Ahmad Kassem,[2] Magali Allain,[2] Maria Paula Duarte,[3] Carlos Lodeiro,[1,4,5] Clément Cabanetos,[2,*] Elisabete Oliveira,[1,4,5,*]

[1] BIOSCOPE Research Group, LAQV-REQUIMTE, Chemistry Department, NOVA School of Science and Technology, Universidade NOVA de Lisboa, 2829-516 Caparica, Portugal; [2] CNRS, MOLTECH-ANJOU, SFR-MATRIX, F-49000 Angers, France; [3] MEtRICs / NOVA School of Science and Technology, Universidade NOVA de Lisboa, Campus de Caparica, 2829-516, Caparica, Portugal; [4] Canterbury Christ Church University, School of Human and Life Sciences, Life, Sciences Industry Liaison Lab, Sandwich, UK; [5] PROTEOMASS Scientific Society, 2825-466, Costa de Caparica, Portugal

Received: March 2025 **Accepted:** April 2025 **Available Online**: June 2025

Abstract

Given the growing concern over antimicrobial resistance (AMR), the search for new alternative therapeutic strategies has increased, with antimicrobial photodynamic therapy (aPDT) emerging as a promising solution. This study aims at exploring the potential of two positively charged Benzothioxanthene imide derivatives (BTI) derivatives, namely BTI-Pyr$^+$-CH$_3$ (**C1**) and DBI-Pyr$^+$-CH$_3$ (**C2**) as photosensitizers for aPDT. In this context, **C1** and **C2** were successfully synthesized, fully characterized, and their antibacterial activity against Gram-negative and Gram-positive bacteria evaluated. The results demonstrate that both compounds exhibit phototoxic effects under light exposure, with enhanced inhibitory and bactericidal activity at lower concentrations than those reported in the existing literature. Notably, Compound **C1** displayed the most promising antibacterial effects, showing inhibitory activity at concentrations approximately 20 times lower than those previously reported. The study highlights the significant light-dependent antibacterial properties of these affordable and accessible compounds, particularly against Gram-positive bacteria, suggesting a potential use for future antimicrobial applications.

Keywords: Antimicrobial Photodynamic Therapy (aPDT); Benzothioxanthene imide derivatives (BTI); Bacteria.

Introduction

The increase of antimicrobial resistance (AMR) mechanisms throughout commonly occurring bacterial colonies is becoming an alarming public health concern [1]. The new Global Research Agenda for Antimicrobial Resistance in Human Health, developed by the World Health Organization (WHO) [2], emphasizes the need for prevention strategies that aim to prevent infections before they occur. This guideline not only reduces the need for antibiotic use but also helps slow the spread of resistance mechanisms in microorganisms present in both domestic and clinical environments. This approach focuses on inhibiting or inactivating microorganisms before they can infect a human host, preventing the onset of the infectious process.

A promising alternative that has gained attention is the use of antimicrobial photodynamic therapy (aPDT) [3]. This process is based on a light-dependent oxygen-dependent photochemical reaction, used to, *in situ*, generate reactive oxygen species (ROS). In the context of PDT, two ROS can be formed through two distinct fundamental mechanisms: Type I and II. Type I is commonly characterized by the production of radicals through electron/hydrogen transferences, yielding superoxide anions that can subsequently be transformed into more reactive ROS. On the other hand, the direct production of singlet oxygen through energy transfer typically characterizes Type II [4]. Both mechanisms can produce a significant antimicrobial effect, serving as an effective alternative to traditional antibiotics. However, while aPDT has a broad range of potential applications, most studies in the literature focus primarily on its use as an anticancer treatment, as well as in dentistry and dermatological applications [5–8].

Benzothioxanthene imide (BTI), a sulfur-containing rylene imide dye, has recently emerged as a highly promising alternative to state-of-the-art photosensitizers for PDT. Its unique chemical structure allows for efficient light absorption and precise modulation of its optoelectronic properties. Upon specific functionalization of its π-conjugated backbone, the selective generation of reactive oxygen species (ROS I and/or ROS II) has been demonstrated [9,10]

***Corresponding author:** clement.cabanetos@univ-angers.fr (CC) and ej.oliveira@fct.unl.pt (EO)

making it an excellent candidate for photonics and biophotonics applications, particularly in PDT [11,12].The compound's high photostability and strong fluorescence further enhance its potential for both therapeutic and diagnostic purposes, enabling targeted treatments with minimal damage to healthy tissue [13]. As a versatile photosensitizer, BTI holds considerable promise for advancing non-invasive, targeted therapies in areas such as cancer treatment; however, its antimicrobial properties and applications remained, to date, unexplored. It is in this precise context that we present the synthesis, characterization, and evaluation of this family of compounds as potential photosensitizers for antimicrobial photodynamic therapy (aPDT). Prepared with minimal synthetic efforts, through a straightforward route, two positively charged derivatives were tested, under light and dark incubation conditions, against a broad spectrum of Gram-positive and Gram-negative bacterial strains. The obtained results in this study confirmed the high potential of such structures with promising and selective phototoxicity.

Materials and Methods

Chemicals and Starting Materials

Mueller-Hinton Broth (MHB), Mueller-Hinton Agar (MHA) and Tryptone Soy Agar (TSA) were acquired from Biokar. Sodium Chloride was purchased from Sigma Aldrich. The **BTI**, **BTI-Br** and **DBI** were prepared from the literature [11,14,15]. Chemicals, reagents and solvents used for the preparation of both **BTI-Pyr$^+$-CH$_3$** and **DBI-Pyr$^+$-CH$_3$** were purchased from Sigma Aldrich. Thin Layer Chromatographies (TLCs) were performed on pre-coated aluminium sheets with 0.20 mm Merck Alugram SIL G/UV254 under UV @ 254nm. Column chromatography purifications were carried out using Sigma-Aldrich silica gel 60 (particle size 63-200 µm). Lab Armor™ beads were purchased from Thermo Fisher Scientific.

Instrumentation

Nuclear magnetic resonance (NMR) ^{1}H and ^{13}C spectra were obtained on a Bruker 300 MHz Avance III spectrometer (300 MHz for ^{1}H and 75 MHz for ^{13}C), on a Bruker 500 MHz Avance III HD spectrometer (500 MHz for ^{1}H and 125 MHz for ^{13}C) and on a Bruker 600 MHz Avance III HD spectrometer (600 MHz for ^{1}H and 151 MHz for ^{13}C). Chemical shifts were reported in ppm according to tetramethylsilane using the solvent residual signal as an internal reference ($CDCl_3$: δH = 7.26 ppm, δC = 77.16 ppm and DMF-d_7 : δH = 8.03 ppm, δC = 163.13 ppm). Coupling constants (J) were given in Hz. NMR spectra were measured at 25ºC. Resonance multiplicity was described as s (singlet), d (doublet), t (triplet), m (multiplet), dd (doublet of doublets), tt (triplet of triplets), td (triplet of doublets), and br (broad signal). Carbon spectra were acquired with a complete decoupling for the proton. High resolution mass spectrometry (HRMS) was performed with a JEOL JMS-700 B/E. Crystal data were collected on a Rigaku Oxford Diffraction SuperNova diffractometer equipped with an Atlas CCD detector and micro-focus Cu-K_α radiation (λ = 1.54184 Å). The structures were solved by dual-space algorithm and refined on F2 by full matrix least-squares techniques using SHELX package (G.M. Sheldrick, ShelXL2019/3). All non-hydrogen atoms were refined anisotropically, and the H atoms were included in the calculation without refinement. Multiscan empirical absorption was corrected by using CrysAlisPro program (CrysAlisPro, Rigaku Oxford Diffraction, V1.171.41.118a, 2021). Deposition Number(s) 2428516 (for **BTI-Pyr**) and 2428517 (for **DBI-Pyr**) contain(s) the supplementary crystallographic data for this paper. This data is provided free of charge by the joint Cambridge Crystallographic Data Centre and Fachinformationszentrum Karlsruhe Access Structures service.

Antibacterial assays were conducted under asepsis conditions, ensured by a STERIL-VBH Laminar Flux Chamber. Incubations were conducted in a Mermmet Incubator B10. Sterile, single-use loops, transparent clear bottom 96-well plates were acquired from Greiner Bio-One. Bacterial suspension concentrations were adjusted with a Densitometer DEN-1B (Grant-Bio).

Synthesis of compounds

BTI-Pyr: To an oven dried Schlenk tube containing a stirring bar, **BTI-Br** (200 mg, 0.442 mmol), pyridin-4-ylboronic acid (81 mg, 0.663 mmol), $Pd(PPh_3)_4$ (50 mg , 0.044 mmol) and K_2CO_3 (183 mg, 1.3 mmol) were sequentially added. The solids were degassed 3 times under vacuum followed by a flow of argon. After addition of degassed dioxane and water (7:1 V:V ratio) the reaction mixture was heated to 110 °C in a bath of Lab Armor™ beads for 4 hours. After cooling down to room temperature, the mixture was diluted with dichloromethane (approx. 30 mL), transferred into a decantation flask where it was washed with water (3x30mL). Organic phases were then dried over $MgSO_4$ before being concentrated under vacuum. The crude was finally purified by column chromatography on silica gel using $CHCl_3$/MeOH (99:1) as eluent to afford BTI-Pyr as a yellow-orange solid (185 mg, 93%). **^{1}H NMR (300 MHz, $CDCl_3$)** δ 8.86 – 8.78 (m, 2H), 8.65 (d, J = 7.9 Hz, 1H), 8.35 – 8.18 (m, 3H), 7.50 – 7.33 (m, 4H), 7.27 (m, 1H) 5.06 (m, 1H), 2.34 – 2.14 (m,2H), 1.98 – 1.83 (m, 2H), 0.95 – 0.84 (t, J = 7.5 Hz, 6H). **^{13}C NMR (151 MHz, $CDCl_3$)** δ 150.9, 146.6, 138.3, 136.9, 132.3, 132.3, 132.2, 132.1, 132.0, 131.3, 131.2, 130.1, 128.7, 128.6, 128.0, 127.7, 126.8, 126.1, 126.0, 124.0, 120.0, 57.6, 25.0, 11.4. **HRMS (MALDI-TOF)** m/z: Calculated for $C_{28}H_{22}N_2O_2S$ (M^+) 450.13965; Found 450.13930 (Δ = -0.78 ppm).

BTI-Pyr$^+$-CH$_3$: (30 mg, 0.067 mmol) was dissolved in acetonitrile (6 mL) MW tube equipped with a magnetic stirred. Iodomethane (18 mg, 0.133 mmol) was then added dropwise, and the reaction mixture was heated to 110 °C in a bath of Lab Armor™ beads for 16 hours. The reaction mixture was cooled down to room temperature before evaporating the solvent under reduced pressure. The resulting solid was washed with a mixture of PE/DCM (8:2) to afford a dark red solid (38 mg, 80 %). **^{1}H NMR (600 MHz, DMF-d_7)** δ 9.50 (d, J = 6.1 Hz, 2H), 8.76 (d, J = 8.2 Hz, 1H), 8.70 (d, J = 6.0 Hz, 2H), 8.68 (d, = 8.0 Hz, 1H), 8.63 – 8.60 (m, 1H), 8.35 (s, 1H), 7.76 – 7.70 (m, 1H), 7.60 – 7.55 (m, 2H), 5.06 – 4.99 (m, 1H), 2.30 – 2.19 (m, 2H), 1.96 – 1.86 (m, 2H), 0.89 (t, J = 7.5 Hz, 6H).

^{13}C NMR (151 MHz, DMFd7) δ 206.0, 154.6, 147.1, 138.5, 136.7, 133.9, 133.2, 132.1, 132.1, 131.8, 131.7, 130.9, 130.2, 129.8, 128.9, 128.8, 128.8, 128.7, 128.3, 127.4, 126.9, 126.9, 125.6, 121.5, 57.2, 48.2, 24.7, 10.9. **HRMS (MALDI-TOF)** m/z: Calculated for $C_{29}H_{25}N_2O_2S$ (M^+) 465.16313; Found 465.16290 (Δ = -0.48 ppm).

DBI-Br: To a solution of **DBI** (500 mg, 1.18 mmol) in CH_2Cl_2 (90 mL) was added dropwise a 1 M solution of bromine in CH_2Cl_2 (190 mg, 1.18 mmol). The reaction mixture was refluxed for 16 h before being quenched with a saturated aqueous solution of $Na_2S_2O_3$. The organic phase was washed with water (2x) and brine (1x), dried over $MgSO_4$ and concentrated under reduced pressure. The resulting crude was purified by column chromatography on silica gel using CH_2Cl_2 as eluent to afford the target **DBI-Br** as orange solid (416 mg, 70%). **^{1}H NMR (300 MHz, CDCl$_3$)** δ (ppm) 8.70 – 8.58 (m, 3H), 8.47 (d, J = 8.1 Hz, 1H), 7.90 – 7.81 (m, 2H), 7.58 – 7.50 (m, 2H), 7.46 (d, J = 8.6 Hz, 1H), 5.16 – 5.01 (m, 1H), 2.35 – 2.18 (m, 2H), 2.00 – 1.84 (m, 2H), 0.91 (t, J = 7.5 Hz, 6H).13C NMR (76 MHz, CDCl3) δ (ppm) 136.7, 134.2, 133.0, 131.4, 130.8, 130.2, 129.2, 129.0, 127.7, 127.0, 126.5, 125.1, 124.0, 123.2, 114.1, 77.6, 57.7, 25.0, 11.5. **HRMS (MALDI-TOF)** m/z calculated for $C_{27}H_20BrNO_2S$ (M^+) 501.03926, found: 501.03900 (Δ = -0.57 ppm).

DBI-Pyr: To an oven dried Schlenk tube charged with a stirring bar was loaded DBI-Br (200 mg, 0.398 mmol), pyridin-4 ylboronic acid (73.39 mg, 0.597 mmol), $Pd(PPh_3)_4$ (46 mg , 0.0398 mmol) and K_2CO_3 (105 mg, 0.76 mmol). These powders were exposed to 3 vacuum/argon refilling cycles. Then, degassed dioxane and water (7:1 V:V ratio) were added and the reaction mixture was heated to 110 °C in a bath of Lab Armor™ beads for 5 hours. Cooled down to room temperature, the reaction mixture was diluted with CH_2Cl_2, and the organic phase was washed with water (2x) before being dried over $MgSO_4$, filtered and concentrated under vacuum. The dark crude was finally purified by column chromatography on silica gel using $CHCl_3$/MeOH (99:1) as eluent to afford **DBI-Pyr** as a yellow-orange solid (186 mg, 93%). **^{1}H NMR (500 MHz, CDCl$_3$)** δ 8.82 (d, J = 5.1 Hz, 2H), 8.71 – 8.64 (m, 2H), 8.49 (d, J = 8.1 Hz, 1H), 8.36 (s, 1H), 7.87 (dd, J = 6.2, 3.3 Hz, 1H), 7.80 (d, J = 8.6 Hz, 1H), 7.60 – 7.52 (m, 4H), 7.31 (d, J = 8.5 Hz, 1H), 5.15 – 5.05 (m, 1H), 2.35 – 2.22 (m, 2H), 1.99 – 1.87 (m, 2H), 0.92 (t, J = 7.4 Hz, 6H). **^{13}C NMR (126 MHz, CDCl$_3$)** δ 151.0, 146.6, 138.3, 136.9, 132.3, 132.2, 132.1, 132.0,131.3, 131.2, 130.1, 128.7, 128.6, 128., 127.7, 126.8, 126.1, 126.0, 124.0, 120.0, 57.6, 25.0, 11.4. **HRMS (MALDI)** m/z: calculated for $C_{32}H_{24}N_2O_2S$ (M^+): 500.15530, found: 500.15470.(Δ = -1.13 ppm).

DBI-Pyr$^+$-CH$_3$: the BTI-Pyr precursor (30 mg, 0.060 mmol) was charged in a microwaved reactor and subsequently dissolved in acetonitrile (6 mL) before adding dropwise iodomethane (17 mg, 0.119 mmol) under stirring. The reaction mixture was warmed up to 110 °C in a bath of Lab Armor™ beads and stirred for 24h. Once cooled down to room temperature, the solvent was directly evaporated the resulting powder was washed with a mixture of PE/DCM (8:2) to afford a dark purple solid (36 mg, 93%). **^{1}H NMR (300 MHz, DMF-d$_7$)** δ 9.48 (d, J = 6.1 Hz, 2H), 8.86 – 8.65 (m, 4H), 8.42 (s, 1H), 8.14 (t, J = 7.3 Hz, 2H), 7.72 – 7.68 (m, 2H), 7.66 – 7.60 (m, 2H), 5.24 – 4.93 (m, 1H), 4.75 (s, 3H), 2.36 – 2.20 (m, 2H), 2.00 – 1.85 (m, 2H) , 0.91 (t, J = 7.4 Hz, 6H). 13C NMR (76 MHz, DMF-d7) δ 155.5, 148, 138.7, 137.6, 135.3, 135.1, 133.8, 133, 132.8, 132.7, 132.3, 131.9, 130.8, 130.4, 130.3, 129.8, 129.7, 129.5, 129.1, 128.4, 128.3, 125.9, 125.1, 124.2, 58.1, 49, 25.7, 11.9. **HRMS (MALDI) m/z:** calculated for $C_{33}H_{27}N_2O_2S^+$ (M^+) 515.17878, found: 515.17790 (Δ = -1.68 ppm).

Photophysical Characterization

Stock solutions at a concentration of 10^{-2} M were made for each compound (**BTI-Pyr$^+$-CH$_3$ (C1)** and **DBI-Pyr$^+$-CH$_3$ (C2)**) in MilliQ-H_2O. Absorption, emission and lifetime measurements were conducted using an aqueous solution of the compounds at a concentration of 10^{-5} M, obtained through an appropriate dilution of the stock solution. All spectra were acquired with a room temperature of 25 °C. Luminescent quantum yields were calculated using as a standard an ethanolic solution of fluorescein [Φ = 0.79] [16].

Antibacterial Assays

To determine the antibacterial activity of the compounds, the following strains were selected: *Escherichia coli* (*E. coli*, ATCC® 25922™), *Salmonella enterica* subsp. *Enterica* serovar Cholerasuis (*Salmonella Cholerasuis*, ATCC® 10708™), *Staphylococcus aureus* (*S. aureus*, ATCC® 6538™), and methicillin-resistant *Staphylococcus aureus* (MRSA, ATCC® 33591™). These were evaluated according to broth microdilution protocols, already published by our group [17]. Briefly, a gradient concentration of 95 -0.2 μg/mL for each compound was obtained through successive dilutions in a 96-well plate and incubated with a constant bacterial concentration. These assays were performed under light and dark incubation conditions, with an incubation period of ca. 18 hours. After this incubation period, 5 μL of each well were removed and plated onto a fresh TSA plate and once again incubated overnight under dark conditions to determine bactericidal conditions.

Results and Discussion

Synthesis of BTI-Pyr$^+$-CH$_3$ (C1) and DBI-Pyr$^+$-CH$_3$ (C2)

The synthetic route to both compounds is depicted in **Scheme 1**. Based on a common strategy, both dyes, referred to as BTI and DBI, were initially selectively brominated on the upper naphthalene ring at the alpha position. The effects of the sulfur heteroatom in conjunction with the electron-withdrawing nature of the imide make this position highly reactive towards electrophilic aromatic substitutions thus allowing a straightforward, efficient and selective bromination under mild conditions, using only 1.1 equivalents of bromine at room temperature. The resulting compounds were subjected to a Suzuki-Miyaura cross-coupling reaction with commercially available pyridin-4-ylboronic acid, achieving yields over 90% under optimized conditions established by our group.

The resulting pyridine functionalized compounds (**BTI-Pyr and DBI-Pyr**) were finally quaternized in the presence of iodomethane, in acetonitrile. As the desired charged compounds (**C1** and **C2**) were formed, their limited solubility in acetonitrile caused gradual precipitation, which enhanced their conversion and facilitated their separation from the reaction mixture.

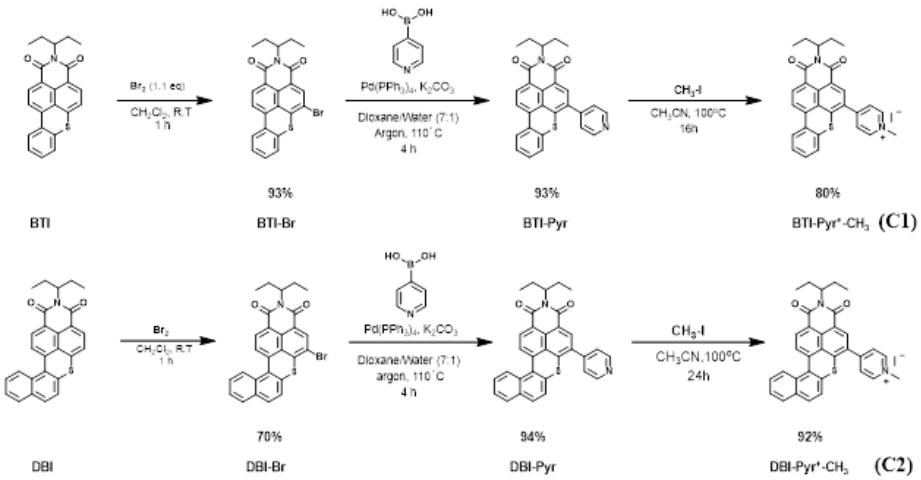

Scheme 1 | Synthetic route to both BTI-Pyr^{+}-CH_3 (**C1**) (top) and DBI-Pyr^{+}-CH_3 (bottom)(**C2**).

Photophysical Characterization

Absorption and emission spectra of both charged compounds, *ie*, **C1** and **C2** were performed in aqueous solutions at 25 ºC, and the main results are depicted in **Figure 1**. Compounds **C1** and **C2** exhibit absorption bands at 478 nm and 504 nm, respectively, and emission bands at 536 and 571 nm. Compound **C1** demonstrates a higher emission quantum yield (Φ = 21 %) compared to **C2** (Φ = 8%). The red shift in the characterization bands of **C2** compared to **C1** was primarily attributed to the presence of an extra aromatic ring in the lower part of the molecule (naphthyl vs phenyl). This additional aromatic ring in **C2** extends the π-conjugation, resulting in a bathochromic shift of about 26 nm in absorption and 35 nm in emission with respect to its phenyl counterpart (**C1**). However, this structural change also results in decreased planarity of the molecule, leading to increased spin orbit coupling and therefore intersystem crossing [11,18]. This instability is also reflected in the lifetime measurements, where **C1** exhibits a longer lifetime, indicating greater stability in the excited state compared to **C2**.

Antibacterial Assays

To assess their antibacterial activity, a broth microdilution assay was selected as it allows for a high-throughput evaluation of inhibitory and bactericidal conditions [19]. To perform this assay, 1 mg/mL aqueous stock solutions were prepared for each compound, and successive dilutions with MHB were performed in a 96-well plate. After the concentration gradients were established, a constant volume of bacterial suspension was added to each well. To determine the influence of light irradiation on the antibacterial activity, two sets of plates were prepared in the same manner. One set was incubated for approximately 18 hours under dark conditions, while the second set was placed in a clear incubator to allow white-light irradiation for the same duration. Biological duplicates were prepared for each tested condition.

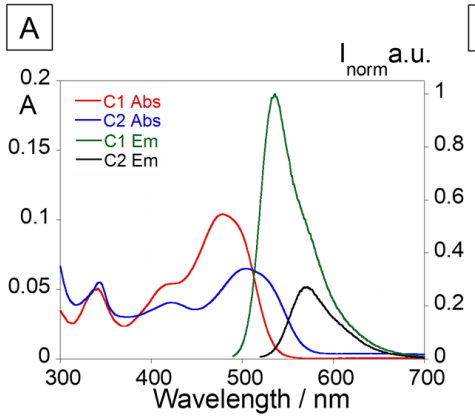

	C1	C2
λ_{abs} (nm)	478	504
λ_{em} (nm)	536	571
Stokes Shift	58	67
Φ (%)	21.3	8.5
τ (ns)	1.919 ± 0.003	1.497 ± 0.014

Figure 1 | Photophysical characterization of compounds **C1** and **C2** (absorption, emission, fluorescence quantum yield and lifetime). Absorption and emission spectra were collected at a sample concentration of 10^{-5} M. ($\lambda_{C1\ exc}$ = 478 nm; $\lambda_{C2\ exc}$= 504 nm; T = 25ºC).

After the incubation cycles, the optical density at 600 nm (OD_{600}) was measured for each well, and data was plotted to correlate sample concentrations with Bacterial Growth percentages, as shown in **Figure 2**. To perform a comparative analysis between the compounds, the Minimum Inhibitory Concentration (MIC), described herein as a decrease of 50% in bacterial growth in the presence of the compound under analysis, was determined (**Figure 2**). To further investigate the antibacterial activity of these compounds, the Minimum Bactericidal Concentration (MBC) was evaluated. An aliquot of 5 µL was removed from each well, plated onto a TSA plate, followed by an overnight incubation period to allow bacterial growth. This step allows for the evaluation of bacterial viability, and, subsequently, the bactericidal activity of compounds, by transferring the bacteria to a medium free of the test compound. If the compound only exerts inhibitory action, bacterial colonies will grow in its absence. Conversely, if the compound demonstrates bactericidal activity, no bacterial growth is expected. To perform a comparative analysis of the antibacterial activity of the compounds, both the MIC and MBC values were determined, as previously described.

A

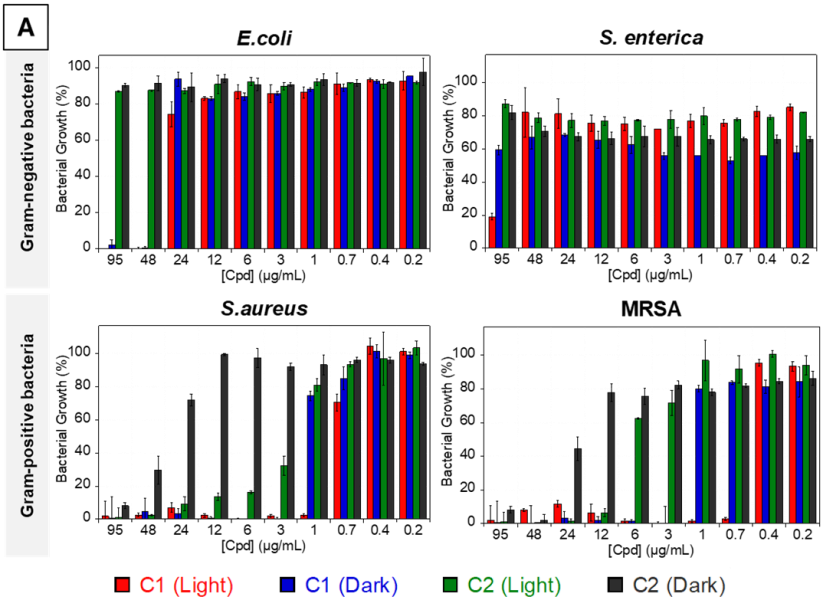

B

Cpd	C1				C2			
Bacteria	Light		Dark		Light		Dark	
	MIC	MBC	MIC	MBC	MIC	MBC	MIC	MBC
E. coli	48	48	48	48	-	-	-	-
Salmonella	95	-	-	-	-	-	-	-
S.aureus	1	3	3	95	3	24	48	-
MRSA	0.7	1	3	-	12	24	24	-

Figure 2 | Bacterial growth profiles (A) of all tested strains, with MIC values (B) represented as compound concentrations (µg/mL).

A clear difference was observed in responses between Gram-positive and Gram-negative bacteria. Regarding the tested Gram-negative bacteria (*E. coli* and *S. enterica*), it was found that only **C1** exhibited significant inhibitory and bactericidal activity. This compound indeed exhibited inhibitory/bactericidal activity against *E. coli* at a concentration of 48 µg/mL, with no observed alterations under light or dark incubation conditions. On contrary, for *S. enterica*, an inhibitory effect was observed at a concentration of 95 µg/mL, with a clear dependence on light irradiation, indicating light sensitivity in this system. Our study also revealed the strong inhibitory effects of both compounds on the tested Gram-positive bacteria (*S. aureus* and MRSA), with a pronounced light-sensitivity. Compound **C1** demonstrated the strongest inhibitory and bactericidal effects against *S. aureus*, with MIC values of 1 and 3 µg/mL under light and dark incubation conditions, respectively. Significant bactericidal effects were also observed in these conditions, with MBC values of 3 and 95 µg/mL, respectively. Regarding **C2**, it also exhibited inhibitory and bactericidal effects with notable modulation in presence of light since MIC of 3 µg/mL were measured under irradiation compared to 48 µg/mL in the dark. Similar results were obtained for MRSA, with **C1** showing inhibitory effects at 0.7 and 3 µg/mL under light and dark conditions, respectively, 12 and 24 µg/mL were determined for **C2**. These findings thus underscore the potential applications of these compounds in light-sensitive environments.

The antibacterial properties of compounds containing the pyridine moiety are well-documented in the literature, with various proposed mechanisms of action [20]. However, the compounds tested here demonstrated improved inhibitory and bactericidal effects at lower concentrations compared to those reported in the

literature. For instance, compared to other pyridine-based compounds that exhibited inhibitory activity at concentrations of 32 μg/mL against *S. aureus* [21], **C1** showed similar inhibitory effects at concentrations approximately 20 times lower. Moreover, both compounds tested here showed significant inhibitory effects against MRSA, competitive with those reported in the literature where pyridine-based compounds had MICs ranging from 32 to 512 μg/mL, substantially higher than the values determined for the compounds tested herein [22]. While further studies are needed to fully understand the antibacterial mechanisms of these compounds, they exhibit promising antibacterial behavior, particularly modulated by light irradiation.

Concluding remarks

By confirming the potential of benzothioxanthene imide derivatives as effective photosensitizers for antimicrobial photodynamic therapy (aPDT), this study presents new design principles, aimed at enhancing efficacy and selectivity. Both compounds **C1** and **C2** exhibit significant antibacterial effects, with **C1** showing superior performances, especially against Gram-positive bacteria, under light irradiation. These findings indicate that this simple, yet readily accessible compound holds great promise for further development as a novel antimicrobial agent, offering a potential solution to combat antibiotic-resistant bacterial strains. Its applicability could extend to both medical and environmental settings to both treatment and prevention.

Acknowledgements

This work was supported by the Associate Laboratory for Green Chemistry - LAQV which is financed by national funds from FCT/MCTES (LA/P/0008/2020 DOI 10.54499/LA/P/0008/2020, UIDP/50006/2020 DOI 10.54499/UIDP/50006/2020 and UIDB/50006/2020 DOI 10.54499/UIDB/50006/2020) as well as the Scientific Society PROTEOMASS (Portugal) for funding support (General Funding Grant 2023-2024). J.G. thanks FCT/MEC (Portugal) for her doctoral grant 2022.09495.BD. E.O thanks FCT/MEC (Portugal) for the individual contract, CEECIND/05280/2022. The MITI, from CNRS, is acknowledged for the PhD grants of both A.K and D.P.S. C.L thanks to the Royal Society of Chemistry (RSC) by the Sustainable Laboratories Grant 2023 (Reference L23-8861107285)

References

[1] Salam MA, Al-Amin MY, Salam MT, Pawar JS, Akhter N, Rabaan AA, Alqumber MAA. Antimicrobial Resistance: A Growing Serious Threat for Global Public Health. Healthcare 2023;11:1946. https://doi.org/10.3390/HEALTHCARE11131946.

[2] Publication Item n.d. https://www.who.int/publications/i/item/9789240102309 (accessed March 16, 2025).

[3] Piksa M, Lian C, Samuel IC, Pawlik KJ, Samuel IDW, Matczyszyn K. The role of the light source in antimicrobial photodynamic therapy. Chem Soc Rev 2023;52:1697–722. https://doi.org/10.1039/D0CS01051K.

[4] Sperandio FF, Huang Y-Y, Hamblin MR. Antimicrobial Photodynamic Therapy to Kill Gram-negative Bacteria. Recent Pat Antiinfect Drug Discov 2013;8:108. https://doi.org/10.2174/1574891X113089990012.

[5] Rajesh S, Koshi E, Philip K, Mohan A. Antimicrobial photodynamic therapy: An overview. J Indian Soc Periodontol 2011;15:323. https://doi.org/10.4103/0972-124X.92563.

[6] Zhou Z, Song J, Nie L, Chen X. Reactive Oxygen Species Generating Systems Meeting Challenges of Photodynamic Cancer Therapy. Chem Soc Rev 2016;45:6597. https://doi.org/10.1039/C6CS00271D.

[7] Almenara-Blasco M, Pérez-Laguna V, Navarro-Bielsa A, Gracia -Cazaña T, Gilaberte Y. Antimicrobial photodynamic therapy for dermatological infections: current insights and future prospects. Frontiers in Photobiology 2024;2. https://doi.org/10.3389/FPHBI.2024.1294511.

[8] Gholami L, Shahabi S, Jazaeri M, Hadilou M, Fekrazad R. Clinical applications of antimicrobial photodynamic therapy in dentistry. Front Microbiol 2023;13. https://doi.org/10.3389/FMICB.2022.1020995.

[9] Saczuk K, Kassem A, Dudek M, Sánchez DP, Khrouz L, Allain M, Welch GC, Sabouri M, Monnereau C, Josse P, Cabanetos C, Deiana M. Organelle-Specific Thiochromenocarbazole Imide Derivative as a Heavy-Atom-Free Type I Photosensitizer for Biomolecule-Triggered Image-Guided Photodynamic Therapy. J Phys Chem Lett 2025:2273–82. https://doi.org/10.1021/acs.jpclett.5c00136.

[10] Puchán Sánchez D, Josse P, Plassais N, Park G, Khan Y, Park Y, Seinfel M, Guyard A, Allain M, Gohier F, Khrouz L, Lungerich D, Ahn HA, Walker B, Monnereau C, Cabanetos C, Le Bahers T. Driving Triplet State Population in Benzothioxanthene Imide Dyes: Let's twist! Chemistry – A European Journal 2024;30:e202400191. https://doi.org/10.1002/CHEM.202400191.

[11] Deiana M, Castán JMA, Josse P, Kahsay A, Puchan-Sánchez D, Morice K, et al. A new G-quadruplex-specific photosensitizer inducing genome instability in cancer cells by triggering oxidative DNA damage and impeding replication fork progression. Nucleic Acids Res 2023;51:6264–85. https://doi.org/10.1093/NAR/GKAD365.

[12] Deiana M, Josse P, Dalinot C, Osmolovskyi A, Marqués PS, Castán JMA, Gillet N, Ravindranath R, Patel AM, Sengupta P, Obi I, Rodríguez-Marquez E, Khrouz L, Dumont E, Abad-Galán L, Allain M, Walker B, Ahn HS, Maury O, Blanchard P, Le Bahers T, Ohlund D, von Hofsten J, Monneraru C, Cabanetos C, Sabouri N. Site-selected thionated benzothioxanthene chromophores as heavy-atom-free small-molecule photosensitizers for photodynamic therapy. Communications Chemistry 2022 5:1 2022;5:1–11. https://doi.org/10.1038/s42004-022-00752-x.

[13] Sánchez DP, Morice K, Mutovska MG, Khrouz L, Josse P, Allain M, Gohier F, Blanchard P, Monnereau C, Le Bahers T, Sabouri N, Zagranyarski Y, Cabanetos C, Deiana M Demadrille R, Welch GC, Risko C, Blanchard P, Cabanetos C. Heavy-atom-free π-twisted photosensitizers for fluorescence bioimaging and photodynamic therapy. J Mater Chem B 2024;12:8107–21. https://doi.org/10.1039/D4TB01014K.

[14] Josse P, Li S, Dayneko S, Joly D, Labrunie A, Dabos-Seignon S, Allain M, Siegler B, . Bromination of the benzothioxanthene Bloc: toward new π-conjugated systems for organic electronic applications. J Mater Chem C Mater 2018;6:761–6. https://doi.org/10.1039/C7TC05245F.

[15] Josse P, Morice K, Puchán Sánchez D, Ghanem T, Boixel J, Blanchard P, Cabanetos C. Revisiting the synthesis of the benzothioxanthene imide five decades later. New Journal of Chemistry 2022;46:8393–7. https://doi.org/10.1039/D2NJ00955B.

[16] Kellogg RE, Bennett RG. Radiationless Intermolecular Energy Transfer. III. Determination of Phosphorescence Efficiencies. J Chem Phys 1964;41:3042–5. https://doi.org/10.1063/1.1725672.

[17] Galhano J, Kurutos A, Dobrikov GM, Duarte MP, Santos HM, Capelo-Martínez JL, Lodeiro C, Oliveira E. Fluorescent polymers for environmental monitoring: Targeting pathogens and metal contaminants with naphthalimide derivatives. J Hazard Mater 2024;480:136107. https://doi.org/10.1016/J.JHAZMAT.2024.136107.

[18] Lodeiro C, Capelo JL, Mejuto JC, Oliveira E, Santos HM, Pedras B, Nuñez C. Light and colour as analytical detection tools: A journey into the periodic table using polyamines to bio-inspired systems as chemosensors. Chem Soc Rev 2010;39:2948–76. https://doi.org/10.1039/B819787N.

[19] Galhano J, Marcelo GA, Duarte MP, Oliveira E. Ofloxacin@Doxorubicin-Epirubicin functionalized MCM-41 mesoporous silica–based nanocarriers as synergistic drug delivery tools for cancer related bacterial infections. Bioorg Chem 2022;118:105470. https://doi.org/10.1016/j.bioorg.2021.105470.

[20] Marinescu M, Popa CV. Pyridine Compounds with Antimicrobial and Antiviral Activities. International Journal of Molecular Sciences 2022, Vol 23, Page 5659 2022;23:5659. https://doi.org/10.3390/IJMS23105659.

[21] Chandak N, Kumar S, Kumar P, Sharma C, Aneja KR, Sharma PK. Exploration of antimicrobial potential of pyrazolo[3,4-b] pyridine scaffold bearing benzenesulfonamide and trifluoromethyl moieties. Medicinal Chemistry Research 2013;22:5490–503. https://doi.org/10.1007/S00044-013-0544-1.

[22] Liu H Bin, Tang H, Yang D, Deng Q, Yuan LJ, Ji QG. Synthesis and biological evaluation of novel N-acyl substituted quinolin-2 (1H)-one derivatives as potential antimicrobial agents. Bioorg Med Chem Lett 2012;22:5845–8. https://doi.org/10.1016/J.BMCL.2012.07.08